PAUL SCHERRER INSTITUT	SLS-2
Magnetic field of longitudinal gradient bend	Document identification SLS2-AM84-001-3
Author(s) M. Aiba, M. Ehrlichman, A. Streun	October 30, 2017

#### Abstract

The longitudinal gradient bend is effective to reduce the natural emittance in light sources. It is, however, not a common element. We analysed its magnetic field and derived a set of formulae. Based on the derivation, it is discussed how to model the longitudinal gradient bend in accelerator codes that are used for designing the electron storage ring. Strengths of multipole components can also be evaluated from the fomulae, and we evaluated the impact of higher order multipole components in a very low emittance lattice.

## Keywords:

Electron storage ring Low emittance lattice Longitudinal gradient bend

### 1. Introduction

New or upgraded third generation light sources will realise small electron beam emittance of pico-meter regime, delivering high brightness photon beams for the experiments. A multi-bend achromat (MBA) lattice, where multiple dipole bending magnets per arc are installed, is generally applied, since the beam emittance is inversely proportional to the third power of the deflection angle per dipole magnet. As the name suggests, the dispersion function is suppressed at both ends so as not to enlarge the electron beam size due to the energy spread at the location of insertion devices.

The optical functions over the dipole magnet are adjusted to lower the emittance. The  $\mathcal{H}$ -function is taken as a figure of merit [1]:

$$\mathcal{H} = \gamma \eta^2 + 2\alpha \eta \eta' + \beta \eta'^2,\tag{1}$$

where  $\beta$ ,  $\alpha$  and  $\gamma$  are Twiss parameters, and  $\eta$  and  $\eta'$  are the dispersion function and its derivative. The amount of emittance generated by photon emission in the bending magnets is proportional to  $\mathcal{H}$ : the smaller  $\mathcal{H}$ , the smaller the beam emittance.

The optimum optical parameters to minimize the  $\mathcal{H}$  function, resulting in the theoretical minimum emittnace, can be analytically found at least for homogeneous dipole field [2]. The minimisation of  $\mathcal{H}$  requires rather small beta and dispersion functions through the dipole magnets, and these values are determined by the length of the dipole magnet. However, they are not realized in practice because too strong focus and/or too long arc length are required, and thus the beam emittance is normally well above the theoretical minimum emittance.

The longitudinal gradient bend (LGB), in which the magnetic field varies along the beam orbit, is effective to reduce  $\mathcal{H}$  and the resulting beam emittance. Several studies can be found in the literature, e.g. [3, 4, 5, 6]. Intuitively, the emittance is lowered when more bending is applied at the location of low dispersion since the emission of synchrotron radiation photon increases the betatron oscillation amplitude, depending on the magnitude of the energy loss and the dispersion function. Therefore, the optimum field profile has a peak in the middle of the dipole magnet [7].

Accelerator codes such as MADX, Bmad and Elegant, are widely used to design storage ring lattices. An LGB, however, is not yet a common accelerator element, and thus it is not available in these codes. We have analysed an LGB's magnetic field and derived a set of formulae to model it properly. In this paper, we report on the analysis and discuss the LGB's multipole components, namely sextupole and octupole. In [6], they are only qualitatively discussed whereas we evaluated the impact of these higher order terms quantitatively.

# 2. Magnetic field description

### 2.1. Coordinate system and magnetic field

The coordinate system shown in Fig. 1 is used throughout this paper. The coordinate of the magnet is represented by fixed Cartesian coordinates, X-Y-Z. The plane X-Z corresponds to the dipole symmetry plane where the horizontal magnetic field components are zero,  $B_X = B_Z = 0$ . On this plane, the vertical field component is given by

$$B_Y = B_Y (X, Y = 0, Z)$$
. (2)

The symbol  $B_Y$  will be used as the vertical field on the symmetry plane, and Y = 0 is omitted hereafter.

The design closed orbit of the beam is normally on the symmetry plane. We employ another coordinate system, x-y-s, moving along the closed orbit. The axis s points in the direction of the beam. The axis s is always parallel to the magnet axis s while the other axes are rotated by the angle between s and s axes, s. The sign of s is defined such that the projection of the axis s to the axis s is pointing to negative s when the angle is positive.

It is convenient to set the origin of the X-Y-Z system to a point where the axis s coincides with the axis z, i.e.  $\theta = 0$  there. Such a point is uniquely determined once the axis z is defined unless the vertical field component  $B_Y$  alters as in undulators, for example. Without loss of generality, we employ a symmetric LGB, i.e.  $\theta = 0$  in the middle of LGB, which can be the origin, and  $B_Y(z) = B_Y(-z)$ .

## 2.2. Multipole expansion

The magnetic field is generally expanded into Taylor series, and the multipole components are directly related to the series terms one by one. We use the following definitions throughout the paper:

$$B_y = \sum_{n=0}^{\infty} \frac{B_n x^n}{n!},\tag{3}$$

and the corresponding multipole strengths are

$$K_n = \frac{B_n}{B\rho},\tag{4}$$

where  $B\rho$  is the magnetic rigidity of the beam. The number of poles is 2(n+1), i.e. n=0 for the dipole field.

The above expansion is defined in the moving coordinate system since the magnetic field acts on the beam particle following the closed orbit with small transverse deviation.

Let us take an arbitrary location on the closed orbit, which we denote by  $(X_0, Z_0)$ . The two coordinate systems are then connected as

$$Z - Z_0 = x \sin \theta_0, \tag{5}$$

and

$$X - X_0 = x \cos \theta_0, \tag{6}$$

where  $\theta_0$  is the angle between the Z and s axes at  $(X_0, Z_0)$ . Hence we get

$$B_0 = B_Y(X_0, Z_0) (7)$$

$$B_1 = \frac{\partial B_Y}{\partial X} \Big|_{X_0, Z_0} \cos \theta_0 + \frac{\partial B_Y}{\partial Z} \Big|_{X_0, Z_0} \sin \theta_0, \tag{8}$$

$$B_2 = \frac{\partial^2 B_Y}{\partial X^2} \Big|_{X_0, Z_0} \cos \theta_0 + \frac{\partial^2 B_Y}{\partial Z^2} \Big|_{X_0, Z_0} \sin \theta_0, \tag{9}$$

$$B_3 = \frac{\partial^3 B_Y}{\partial X^3} \Big|_{X_0, Z_0} \cos \theta_0 + \frac{\partial^3 B_Y}{\partial Z^3} \Big|_{X_0, Z_0} \sin \theta_0, \tag{10}$$

and so on. The first terms in  $B_n$  (n > 0) originate at the transverse gradient, and the second terms originate at the longitudinal gradient. It is shown here that the longitudinal gradient generates the components higher than dipole.

When the transverse gradient terms are zero, the magnetic field of LGB is "rectangular-bend-like" field, where the field contour lines are parallel to the axis X. A special case "sector-bend-like" field, where the contour lines are parallel to the axis x is discussed later although the rectangular-bend-like magnet may be preferable from the manufacturing point of view.

### 2.3. Feed up

The so-called *natural focusing* in the horizontal plane comes from the geometric nature of sector bend magnets. It is naively expected that a focusing is due to a transverse gradient. However, the path length of a particle traveling off closed orbit is longer or shorter than that of the ideal particle on the closed orbit in a sector bend magnet. The bending angle depends on the particle path, and thus the natural focusing arises from a pure dipole field. This applies to the quadrupole component too, i.e., the quadrupole component included in a sector bend generates sextupolar focusing. The quadrupole component discussed here originates not only from the transverse gradient but also from the longitudinal one. Feed up refers to this process whereby an n-th generates an (n+1)-th term.

We now discuss an infinitely short segment of a sector bend magnet to formulate the "feed up" described above. For the short segment, the vertical field,  $B_Y$ , is constant along s but depends on x.

The path length of a particle along the segment is

$$l = (\rho_0 + x)\,\varphi_0,\tag{11}$$

where  $\rho_0$  is the bending radius and  $\varphi_0$  is the bending angle of the segment for the particle on the closed orbit. For the off-closed-orbit particles, the deflection angle is

$$\varphi = B_{Y}l$$

$$= \left(B_{0} + B_{1}x + \frac{B_{2}}{2}x^{2} + \frac{B_{3}}{6}x^{3} + \cdots\right)(\rho_{0} + x)\varphi_{0}$$

$$= B_{0}\rho_{0}\varphi_{0}$$

$$+ B_{0}\varphi_{0}x + B_{1}\rho_{0}\varphi_{0}x$$

$$+ B_{1}\varphi_{0}x^{2} + \frac{1}{2}B_{2}\rho_{0}\varphi_{0}x^{2}$$

$$+ \frac{1}{2}B_{2}\varphi_{0}x^{3} + \frac{1}{6}B_{3}\rho_{0}\varphi_{0}x^{3}$$

$$+ \cdots$$
(12)

The second term corresponds to the natural focusing, and the fourth and sixth terms are the feed up from the quadrupole component to the sextupole component and from the sextupole component to the octupole component, respectively.

### 2.4. Multipole strength

The strength of each component is obtained from Eq. 12 by dividing the length of the segment,  $\rho_o\varphi_0$ , and normalizing to the magnetic rigidity. We now remove the subscript of 0 to represent the strengths as a function of Z and  $\theta$ :

$$K_1(Z) = \frac{B_0(Z)^2}{(B\rho)^2} + \frac{B_1(Z,\theta)}{B\rho},$$
(13)

$$K_2(Z) = \frac{2B_0(Z)B_1(Z,\theta)}{(B\rho)^2} + \frac{B_2(Z,\theta)}{B\rho},$$
 (14)

$$K_3(Z) = \frac{3B_0(Z) B_2(Z, \theta)}{(B\rho)^2} + \frac{B_3(Z, \theta)}{B\rho},$$
(15)

The natural-focusing term (the first term of  $K_1$ ) is normally written as  $1/\rho^2$ . We use, however,  $B_Y^2/(B\rho)^2$  for the convenience of the following integration.

The integrated multipole strengths are found by integrating Eqs. 13–15 along the closed orbit over LGB. The angle  $\theta$  is

$$\theta(s) = \int_0^s \frac{B_Y(s')}{B\rho} ds'. \tag{16}$$

For small bending angles, it is approximately

$$\theta(Z) \approx \int_0^Z \frac{B_Y(Z')}{B\rho} dZ'.$$
 (17)

This approximation is well justified for the low emittance lattice since the deflection angle per dipole magnet is only a few degrees. We assumed that the origin of X-Y-Z is set to the point of  $\theta = 0$ . Otherwise, a constant (the initial angle) should be added to Eq. 17. Hence the integration is simply performed with respect to Z. For an LGB with length of L, the integrated strengths are

$$\int_{0}^{L} K_{1} dZ = \int_{0}^{L} \left[ \frac{B_{0}(Z)^{2}}{(B\rho)^{2}} + \frac{B_{1}(Z)}{B\rho} \right] dZ, \tag{18}$$

$$\int_{0}^{L} K_{2} dZ = \int_{0}^{L} \left[ \frac{2B_{0}(Z) B_{1}(Z)}{(B\rho)^{2}} + \frac{B_{2}(Z)}{B\rho} \right] dZ, \tag{19}$$

$$\int_{0}^{L} K_{3} dZ = \int_{0}^{L} \left[ \frac{3B_{0}(Z)B_{2}(Z)}{(B\rho)^{2}} + \frac{B_{3}(Z)}{B\rho} \right] dZ.$$
 (20)

The expansion coefficients,  $B_n$ , are now a function of Z alone. It is noted that the terms arising from the feed up are important only for the horizontal plane.

For the "sector-bend-like field" (as mentioned previously in Sec. 2.2), the expansion coefficients,  $B_n$ , are zero for n > 0. Therefore, no focusing is expected for the vertical plane while the natural-focusing term still exists in the horizontal plane.

When the magnetic field of LGB quickly falls to zero at the magnet ends, one may simply evaluate the edge focusing separately and add it to the strength of the main field. The linear edge focusing is given by

$$-\frac{\theta_e}{\rho(Z_e)} \quad \text{or} \quad -\frac{B_Y(Z_e)\,\theta_e}{B\rho},\tag{21}$$

where  $\theta_e$  is the edge angle and the magnet end is at  $Z = Z_e$ .

When Eq. 2 is in a form that cannot be analytically integrated, one may rewrite the longitudinal field profile with a polynomial function or a Fourier series since the integral of these bases are easily found. Alternatively, a function which is differentiable several times can be used to represent the profile. Then the multipole strength can be found and integrated numerically.

## 2.5. Linear focusing

When the transverse gradient is zero, Eq. 18 could be integrated differently for the horizontal plane since

$$\int_{0}^{L} K_{1} dZ \approx \int_{0}^{L} \left[ \frac{B_{Y} (Z')^{2}}{(B\rho)^{2}} + \frac{\frac{\partial B_{Y}}{\partial Z} \Big|_{Z'} \theta (Z')}{B\rho} \right] dZ', \tag{22}$$

where an approximation of  $\sin \theta \approx \theta$  is employed. Noting that  $\int (g'^2 + g''g) = g'g$  for a function g,

$$\int_{0}^{L} K_{1} dZ = \frac{B_{Y}(L) \theta(L)}{B \rho}.$$
(23)

From Eq. 23, no horizontal focus is expected when the magnetic field  $B_Y$  reaches to zero at the magnet end. Also, when the magnetic field  $B_Y$  has a sharp edge and the magnet end is parallel to the axis X, the edge focus (Eq. 21) cancels out the horizontal focusing of Eq. 23.

## 3. Analysis of typical field profile

We apply the derived fomulae to typical field profiles, namely a linear profile and a hyperbolic profile.

### 3.1. Linear profile

The magnetic field of a linear (falling) profile with no transverse gradient is given by

$$B_Y(Z) = B_m(1 - Z/L) \quad \text{for} \quad 0 \le Z \le L, \tag{24}$$

$$B_Y = 0 \quad \text{for} \quad Z > L, \tag{25}$$

where  $B_m$  is the maximum field at Z=0, and L is the half length of the magnet.

We set  $\theta = 0$  at Z = 0 and evaluate Eqs. 18–20.

$$\int_0^Z K_1 dZ' = \left(\frac{B_m}{B\rho}\right)^2 \left(\frac{Z^3}{3L^2} - \frac{Z^2}{L} + Z\right) + \left(\frac{B_m}{B\rho}\right)^2 \left(\frac{Z^3}{6L^2} - \frac{Z^2}{2L}\right),\tag{26}$$

$$\int_0^Z K_2 dZ' = \left(\frac{B_m}{B\rho}\right)^3 \left(-\frac{Z^4}{4L^3} + \frac{Z^3}{L^2} - \frac{Z^2}{L}\right),\tag{27}$$

$$\int_0^Z K_n dZ' = 0 \quad \text{for} \quad n > 2,$$
(28)

where an approximation of  $\sin \theta \approx \theta$  is employed. The underlined terms come from the feed up. It is not surprising that  $\int_0^L K_1 dZ = 0$  for zero initial angle as discussed in Sec. 2.5. When the initial angle is finite, we get the integrated strength corresponding to Eq. 21.

## 3.2. Hyperbolic profile

An LGB with hyperbolic field profile is of interest since it fits well the numerically-found optimum field profile [7]. When the transverse gradients are zero, the magnetic field is given by

$$B_Y(Z) = \frac{B_m}{(1+h|Z|/L)^p} \quad \text{for} \quad |Z| \le L,$$
 (29)

$$B_Y = 0 \quad \text{for} \quad |Z| > L, \tag{30}$$

where  $B_m$  is the maximum field at Z = 0, h and p are the parameters to form hyperbolic function, and L is the half length of the magnet.

We again set  $\theta = 0$  at Z = 0 and evaluate Eqs. 18–20 for the latter half of the magnet  $(Z \ge 0)$ .

$$\int_{0}^{Z} K_{1} dZ' = \frac{B_{m}^{2} L}{h (B\rho)^{2}} F(2p-1) + \frac{p B_{m}^{2} L}{(p-1) h (B\rho)^{2}} [F(2p-1) - F(p)],$$
(31)

$$\int_{0}^{Z} K_{2}dZ' = \frac{2pB_{m}^{3}L}{(p-1)h(B\rho)^{3}} [F(3p-1) - F(2p)] - \frac{p(p+1)B_{m}^{2}}{(p-1)(B\rho)^{2}} [F(2p) - F(p+1)],$$
(32)

$$\int_{0}^{Z} K_{3} dZ' = \frac{-\frac{3p(p+1)B_{m}^{3}}{(p-1)(B\rho)^{3}} [F(3p) - F(2p)]}{\frac{p(p+1)(p+2)B_{m}^{2}L}{(p-1)h(B\rho)^{2}} [F(2p+1) - F(p+2)],$$
(33)

where

$$F(P) \equiv \frac{1 - \left(1 + h\frac{Z}{L}\right)^{-P}}{P}.$$
(34)

When the magnet is left-right symmetric, the strengths of the full magnet are double of Eqs 31–33. Otherwise, the integration should be performed for both sides separately. Since the magnetic field is non-zero at the magnet end, the corresponding edge focusing needs to be added.

### 4. Modeling in accelerator code

As mentioned earlier, LGB magnets are not, generally speaking, straightforward to include in accelerator codes. We may introduce it as a stack of short dipoles: the bending angle of each slice is set to reproduce the longitudinal field profile. Eq. 13 should also be fulfilled with the stack of dipoles. A sector bend may then be used for a short dipole to introduce the natural focusing, which is the first term of Eq. 13. Most accelerator codes are capable of adding a field gradient to the sector bend element, and thus the second term of Eq. 13 can be introduced at

the same time. The higher order terms (Eqs. 14 and 15) can be also introduced if the code is capable to include corresponding higher order gradients. Otherwise, they may be introduced as a zero length element inserted between the short dipoles, or omitted as far as they are negligible, as in the numerical example discussed shortly in Sec. 5.

Alternatively, a stack of short sector bends with adjusted edge angles may be used as an approximation. When all the edges are parallel to the axis X of Fig. 1, there is no net focusing for the horizontal plane. Therefore, such a stack can approximately represent an LGB, which should result in no horizontal focusing as discussed in Sec. 2.5, instead of fulfilling Eq. 13 at each slice as in the aforementioned exact model. This is a convenient approximation during lattice design since we can skip computing the second term of Eq. 13. However, when the higher order terms are significant and need to be included, this approximation might be confusing since the feed-up terms would be evaluated for the non-zero edge angles.

## 5. Impact of higher order terms

We evaluated the impact of higher order terms, namely sextupole and octupole. A low emittance lattice under development for an upgrade of the Swiss Light Source [8] is employed. Figure 3 shows the lattice functions and dipole and quadrupole field for one of 12 arcs.

The lattice includes two types of LGB. One is a superconducting magnet with hyperbolic-like field shape, and the other is a normal conducting magnet with a peak field of about 2 T. Figures 4 and 5 show the field profiles and corresponding integrated field components up to octupole. It is seen that the sextupole components are weak with respect to the chromaticity correction sextupoles with integrated strength on the order of 10 m<sup>-2</sup>.

By introducing sextupole components into the lattice, the chromaticities are shifted only on the order of 0.001 in the horizontal plane and 0.01 in the vertical plane. In addition to the fact that LGB sextupole components are weak, the dispersion function is small along LGB, and thus the impact on the chromaticity is negligible.

The dynamic aperture of the lattice is computed with and without LGB sextupole and octupole components (see Fig. 6). The multipole components of the LGBs are much weaker than the ones included in the lattice except for the octupole components of the superconducting LGB. It may be overestimated by a hyperbolic fit where the peak field reaches about 9 T. Such a high peak field may not be achieved in a real magnet and will be <6 T with less sharp field profile. Nevertheless, the dynamic aperture is not spoiled, and thus we concluded that the impact of LGB multipoles is marginal.

### 6. Conclusion

We derived a set of formulae to describe the magnetic field of longitudinal gradient bends in terms of a multipole expansion. They are applicable to any longitudinal field profile as far as the bending angle is small enough to justify the small angle approximations used in the derivation. For the low emittance lattice in which we are interested, the approximation is well justified. The longitudinal gradient bend would be modeled in the accelerator codes as a stack of short sector bends as discussed in Sec. 4. Higher order components, namely sextupole and octupole, are typically weak because they are attenuated through the projection from the longitudinal

gradient to the transverse gradient. We still evaluated their impact quantitatively with a low emittance lattice, and it turned out to be marginal.

### References

- [1] Helm, R. H. and Lee, M. J. and Morton, P. L. and Sands M., Evaluation of Synchrotron Radiation Integrals, Proc. of Part. Accel. Conf. 1973, 900–901, 1973.
- [2] L. C. Teng, Minimizing the Emittance in Designing the Lattice of an Electron Storage Ring, Fermilab Internal Note, TM-1269, 1992.
- [3] A. F. Wrulich, Overview of 3rd Generation Light Sources, Proc. of Workshop on Fourth Generation Light Sources, SSRL92/02, 1984.
- [4] Guo, J. and Raubenheimer, T., Low emittance  $e^-/e^+$  Storage Ring Using Bending Magnets with Longitudinal Gradient, Proc. of European Part. Accel. Conf. 2002, 1136–1138, 2002.
- [5] Papaphilippou, Y. and Elleaume, P., Analytical Considerations for Reducing the Effective Emittance with Variable Dipole Field Strengths, Proc. of Part. Accel. Conf. 2005, 2086– 2088, 2005.
- [6] C. Wang, Minimum Emittance in Storage Rings with Uniform or Nonuniform Dipoles, Phys. Rev. ST Accel. Beams, 12, 061001, 2009.
- [7] Streun, A. and Wrulich, A., Compact Low Emittance Light Source Based on Longitudinal Gradient Bending Magnets, Nucl. Instrum. and Methods in Phys. Research A, 770, 99–112, 2015.
- [8] Bengtsson, J. and Streun, A., Robust Design Strategy for SLS-2, PSI internal note, SLS2-BJ84-001, 2017.

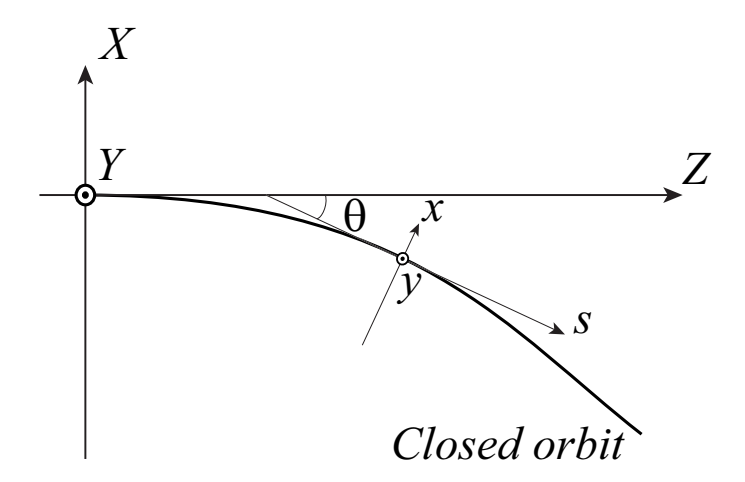


Figure 1: Coordinate system. See text for details.

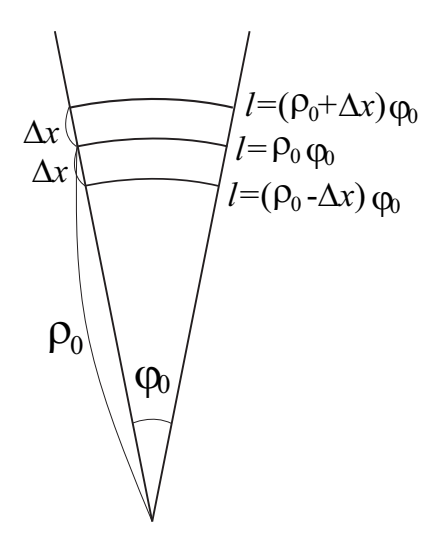


Figure 2: Path length variation in an infinitely short sector bend segment. The path length l depends on the horizontal deviation,  $\Delta x$ .

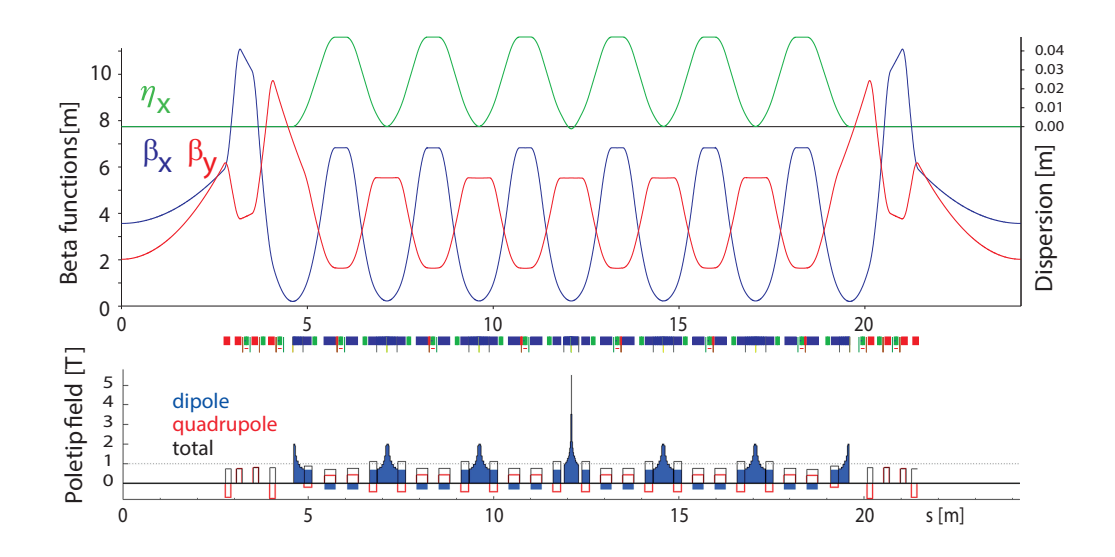


Figure 3: Low emittance lattice for an upgrade of the Swiss Light Source. The circumference is 290.4 m, and the natural emittance is 102 pm. The lattice consists of 12 arcs and 12 straight sections. Nine arcs out of 12 include only normal conducting LGBs while the normal conducting LGB in the middle of the arc is replaced by a superconducting LGB in the other three arcs. Pole tip field corresponds to the one at 13 mm.

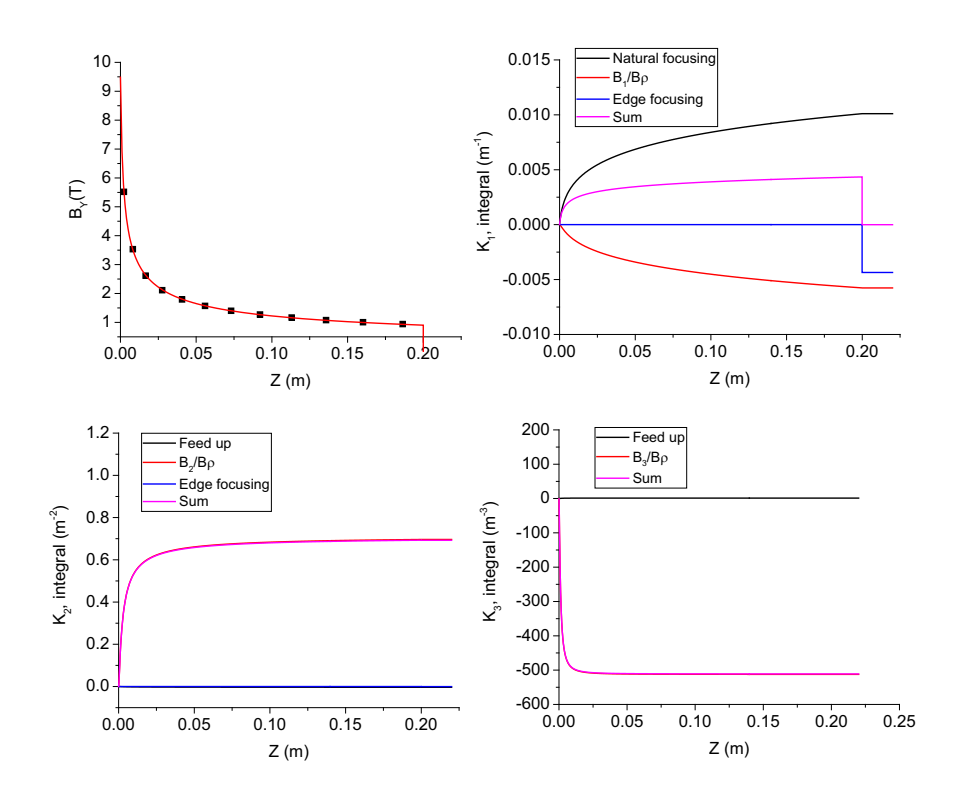


Figure 4: Field profile and integrated multipole components of superconducting LGB. The black dots in the left-top plot show the average field of each stacked short dipole magnet. a hyperbolic function is fitted to the field profile.

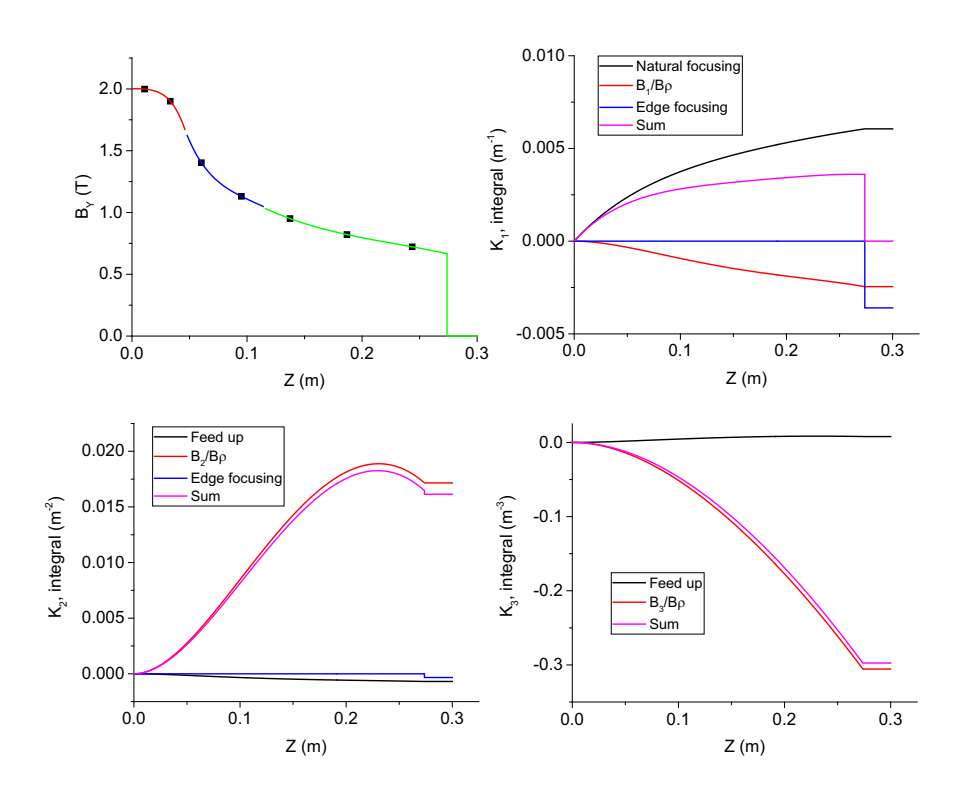


Figure 5: Field profile and integrated multipole components of normal conducting LGB. The black dots in the left-top plot show the average field of each stacked short dipole magnet. A polynomial function is fitted to the field profile. The fitting was applied separately to three different region of the magnet to include only reasonably low order terms (up to 5th order).

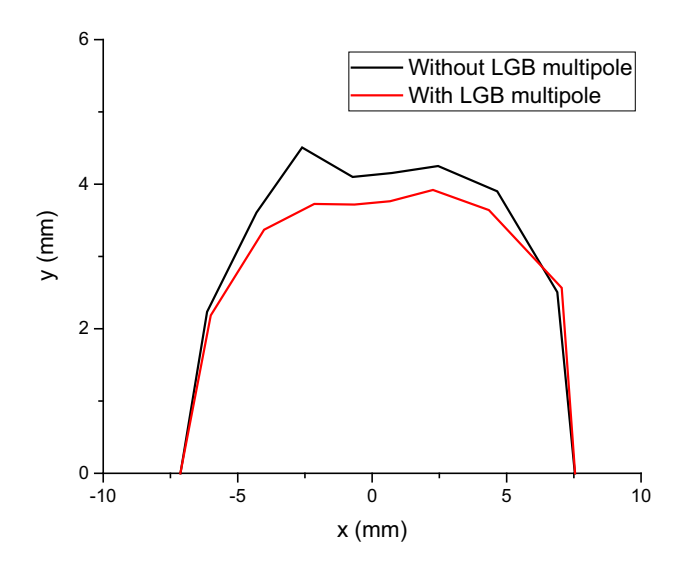


Figure 6: Dynamic aperture with and without LGB multipoles.